Continental Shelf Research 214 (2021) 104323

Contents lists available at ScienceDirect

Continental Shelf Research

journal homepage: http://www.elsevier.com/locate/csr

The impact of sea-level rise and basin area reduction on the cyclic behavior of tidal inlet systems

Klaas J.H. Lenstra [a,b,*], Maarten van der Vegt [a]

[a] Department of Physical Geography, Faculty of Geosciences, Utrecht University, P.O. Box 80.115, 3508TC, Utrecht, The Netherlands
[b] Arcadis, Rivers & Coasts, P.O. Box 220, 3800AE Amersfoort, The Netherlands

ARTICLE INFO

Keywords:
Ebb-tidal deltas
Cyclic behavior
Human impact
Barrier-islands
Sea-level rise

ABSTRACT

Ebb-tidal deltas filter incoming wave energy and mitigate erosion of basins and coasts by temporarily providing sediment. In many systems, these coastal safety functions are under threat from human activities. Here we use Delft3D/SWAN to assess the effects of relative sea-level rise and changes in basin area on the long-term dynamics of ebb-tidal deltas. The results show that the time scales of the cyclic channel-shoal dynamics of ebb-tidal deltas are affected. An instantaneous decrease in basin area slows down the cyclic behavior during the initial adjustment period. The duration of the adjustment period increases with larger basin area reduction. After the adjustment, smaller basins have shorter time scales of cyclic channel-shoal dynamics. This is linked to a decrease in tidal prism and ebb-tidal delta volume. Moreover, we find that the effects of relative sea-level rise depend on the rate of rising water levels. For relatively low rates, the period of the cycles eventually shortens, whereas higher rates can cause longer periods. The volume of ebb-tidal deltas appears to be unaffected by relative sea-level rise; but because the average water depth increases, more energetic waves reach the basin. By showing how ebb-tidal deltas adjust to relative sea-level rise and basin area reduction and by unraveling the underlying mechanisms, this study contributes to our understanding of the long-term evolution of tidal inlets.

1. Introduction

During the last century, anthropogenic activities have disrupted the natural dynamics at many barrier island systems (Stutz and Pilkey, 2005). Human-induced disruptions can be direct (e.g. nourishments, channel dredging, jetty/dike construction) or indirect (climate change, relative sea-level rise). As a result, in the Dutch Wadden Sea, roughly 600 million m^3 of sediment has been deposited in the basin area since 1935, which is linked to erosion of the ebb-tidal deltas (~ 450 million m^3, Elias et al., 2012). Part of the changes in the sediment distribution in the Dutch Wadden Sea is believed to be caused by relative sea-level rise (Van der Spek, 2018; Wang et al., 2018). Moreover, the closure of the Zuiderzee, reducing the Texel and Vlie basin areas by roughly 60%, and the closure of the Lauwerszee, reducing the Frisian Inlet basin area by roughly 30%, resulted in additional sediment import to these basins and also in erosion of the ebb-tidal deltas (Ridderinkhof et al., 2014). These large-scale changes in the sediment balance of the Wadden Sea pose problems for coastal safety for two reasons. Firstly, eroding ebb-tidal deltas lose their ability to absorb wave energy propagating to the coasts and basins (Hansen et al., 2013). Secondly, less sediment is available to balance local erosion of the islands and tidal basins.

Furthermore, observations show that ebb-tidal deltas not only eroded, but also changed their shape and sediment bypassing (Biegel and Hoekstra, 1995; Van de Kreeke, 2006; Ridderinkhof et al., 2016b). For the Wadden Sea, most of the sediment is bypassed through periodic shoal formation, migration and shore attachment accompanied by channel rotation and breaching (e.g. FitzGerald, 1982). However, it is not clear how human intervention changed this cyclic behavior.

Oost (1995) observed that the cyclic behavior had stopped at the Frisian Inlet system after the closure of the Lauwerszee. Because approximately 30% of the surface area of the basin area was closed off, the surplus in ebb-tidal delta sediment formed a substantial shoal, which eventually attached to the downdrift Schiermonnikoog island (Elias et al., 2012). In contrast, channel deflection and breaching were no longer observed on the ebb-tidal delta. However, Ridderinkhof et al. (2016b) observed the formation and migration of a new shoal from 2005 onwards and Elias et al. (2012) suggested that eventually a cyclic development as observed prior to the closure will reappear. However, the time scale of adjustment remains unknown. Furthermore, it is unclear how this cyclic behavior will differ and whether the period

* Corresponding author. Department of Physical Geography, Faculty of Geosciences, Utrecht University, P.O. Box 80.115, 3508TC, Utrecht, The Netherlands.
E-mail address: k.j.h.lenstra@uu.nl (K.J.H. Lenstra).

https://doi.org/10.1016/j.csr.2020.104323
Received 2 May 2020; Received in revised form 9 November 2020; Accepted 3 December 2020
Available online 17 December 2020

between successive shoals will change. Because this period positively correlates with tidal prism (Gaudiano and Kana, 2001; Ridderinkhof et al., 2016b), the smaller ebb-tidal delta and reduced tidal prism render it likely that shoals of smaller volume will attach more frequently and merge closer to the inlet. Also for the nearby Texel and Vlie inlets it remains unclear how the time scale of the cyclic channel-shoal dynamics changed by the closure of the Zuiderzee in 1931 and whether the adjustment has finished. The natural variability in the dynamics makes it difficult to isolate the effect of the basin reduction in these observations or to quantify the adjustment time scale.

This paper considers the most common type of cyclic behavior, which FitzGerald (1988) denoted as ebb-tidal delta breaching. It features three phases, namely channel rotation, shoal growth and channel breaching. Using an idealized mophodynamic model, Lenstra et al. (2019b) showed that the relative importance of waves and tides varies amongst the three phases. Channel rotation is caused by wave-induced currents and sediment concentration, while shoal growth can only be explained by the combined effect of tides and waves. Moreover, there exists an optimum balance between tides and waves for the breaching of the ebb-tidal delta: if the waves are too small, not enough sediment is entrained for the formation of the new channel, whilst too high waves cause further channel rotation rather than channel breaching. This provides an excellent framework to understand how human intervention change the dynamics of ebb-tidal deltas and to discriminate between adaptation behavior and new dynamics because of the changes in geometry.

In addition, the dynamics of tidal inlet systems are also affected by relative sea-level rise (e.g. Dissanayake et al., 2009; Becherer et al., 2018; Vermeersen et al., 2018). Rising mean levels increased the volume of sediment accommodation space and generated is believed to have generated additional sediment import through the inlets in the Wadden Sea (Elias et al., 2012; Van der Spek, 2018). Because especially the shoal formation and growth depends on this sediment exchange between basin and ebb-tidal delta (Lenstra et al., 2019b), relative sea-level rise is likely to result in longer time scales for the cyclic behavior of ebb-tidal deltas. Moreover, if the sediment import is insufficient to let the intertidal flats accrete (drowning of basins, see Wang et al., 2018), changes in tidal prism and tidal wave characteristics are expected (Ridderinkhof et al., 2014). It unknown how the dynamics of ebb-tidal deltas respond to the sea-level-rise-induced changes in sediment import and basin morphology.

Although the examples given above were based on observations and studies covering the Dutch Wadden Sea, the described issues are not limited to this area. Not only is relative sea-level rise a worldwide phenomenon, but also is basin area reduction common practice around the world. For example, there has been land reclamation and/or dike construction in tidal basins in the USA (Hansen et al., 2013; Beck and Kraus, 2011), China (Wang et al., 2014), Australia (Sennes et al., 2007) and Italy (Rizzetto et al., 2009). FitzGerald et al. (1984) showed that poldering behind the barrier islands and along the mainland have reduced the basin areas of the East Frisian inlets (Germany) between 1650 and 1960 by 149 km^2, which is roughly 30% of their original drainage area.

While the time scales of the cyclic behavior (long-term) and the mechanisms and the relative importance of tides and waves throughout the various phases (short-term) are relatively well understood for natural systems (Ridderinkhof et al., 2016a; Lenstra et al., 2019b), it is unknown how this mophodynamic equilibrium is affected by anthropogenic activities. Here, we aim to elucidate how the volume and cyclic behavior of an ebb-tidal delta are affected by (1) an instantaneous reduction in basin size and tidal prism and (2) different rates of relative sea-level rise. The main focus is on the long-term effects, i.e. the time scales of cyclic behavior and the evolution of the volume and wave-filtering capacity of the ebb-tidal delta. These long-term effects will be explained by changes to the known short-term mechanisms. Relative sea-level rise and basin reduction are here considered separately to isolate their individual effects; it is not the aim of this study to understand how the effects of these two disruptions dominate over one another. These questions are addressed using an idealized geometry and simplified forcing in Delft3D/SWAN (Section 2), where we studied the morphodynamics of ebb-tidal deltas for a wide range of basin size reductions and rates of relative sea-level rise. The outcome will be compared in Section 3 with undisturbed model simulations (constant basin size and mean sea level) with clear patterns of channel-shoal dynamics (Lenstra et al., 2019b). The discussion and conclusions are presented in Sections 4 and 5, respectively.

2. Material and methods

The numerical model Delft3D for hydrodynamics, sediment transport and bed level updates (Lesser et al., 2004; Deltares, 2014), coupled with the wave model SWAN (Booij et al., 1999; Ris et al., 1999; Holthuijsen, 2010), was used to investigate the effect of different disturbances on the cyclic behavior of ebb-tidal deltas. Using an idealized geometry and simplified forcing, we studied the disturbed morphodynamic evolution of ebb-tidal deltas for several basin size reductions and relative sea-level rise rates. The results were compared with undisturbed reference model simulations with constant basin size and steady mean water level, based on the simulations presented in Lenstra et al. (2019b). These showed clear patterns of channel-shoal dynamics resembling those observed in tidal inlet systems, and are therefore an ideal starting point to study the effects of human interventions. A brief description of the model setup, forcing and new aspects are provided below; however, for complete details the reader is referred to Lenstra et al. (2019b).

2.1. Model domains and settings

The Delft3D flow module solves the depth-averaged shallow water equations (conservation of mass and momentum balance) to calculate flow velocities and water levels. The rectangular model domain (Fig. 1)

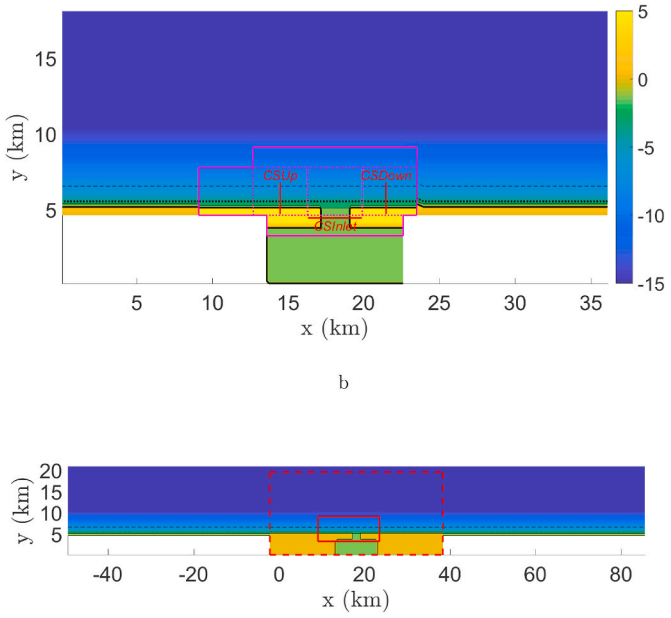

Fig. 1. Domains that are considered in Delft3D (a) and SWAN (b) with colors indicating initial bathymetry. The magenta lines in the Flow domain enclose the grids with highest resolution in the model and the red lines indicate cross-sections used for analysis. The red lines in the wave domain indicate the three nested grids. Note that the basin area for some simulations is different than the one shown here, see Fig. 2. (For interpretation of the references to color in this figure legend, the reader is referred to the Web version of this article.)

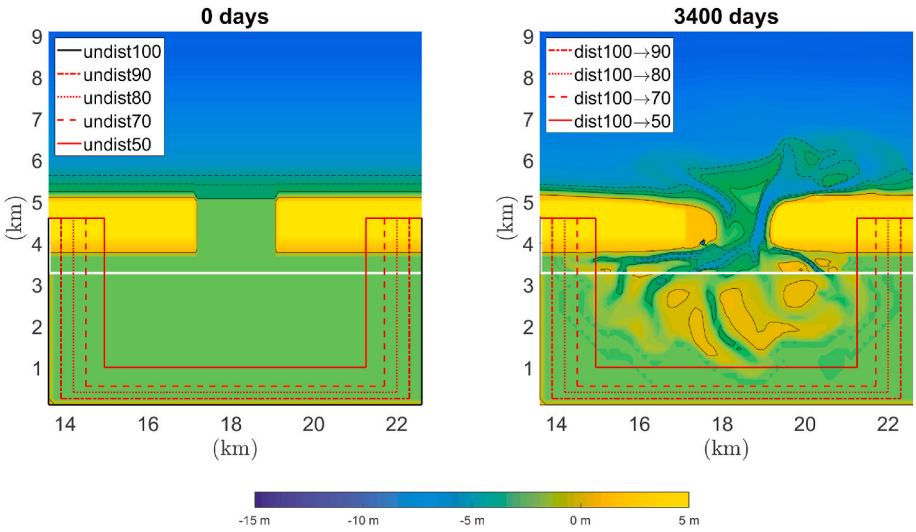

Fig. 2. Starting bathymetries for the undisturbed (left) and disturbed (right) runs. The white line indicates the coupling of the high-resolution domain (grid size 50 m) and the low-resolution domain (150 m). The red lines indicate the areas that were removed from the model domain for the simulations with a reduction in basin area. (For interpretation of the references to color in this figure legend, the reader is referred to the Web version of this article.)

consists of one inlet connecting the open sea to the tidal basin. This study focuses on relatively short basins with a standing tidal wave, such as the Frisian Inlet. The domain is divided into eight two-way coupled domains (domain decomposition) with grid resolutions of $1/50$ m^{-1} for the area of interest (inlet and ebb-tidal delta), $1/150$ m^{-1} for the tidal basin and $1/450$ m^{-1} for the outer sea (Fig. 1). The time step was set at 12 s and the bed roughness was prescribed with a uniform Chézy friction coefficient value of 65 m$^{0.5}$/s. The horizontal eddy diffusivity and viscosity were set at 1 m^2/s and 10 m^2/s, respectively.

The hydrodynamic model was coupled to the third-generation phase-averaged spectral wave model SWAN (coupling time of 60 min), which solves the wave action balance equation. The SWAN model considered wave breaking (formulation of Battjes and Janssen (1978), $\gamma = 0.73$), white-capping (Komen et al., 1984) and bottom friction (JONSWAP). However, it did not account for wind growth, wave diffraction or non-linear triad-interactions. The wave domain consists of three nested grids with decreasing grid resolutions of $1/1350$ m^{-1} (east-west extension to avoid shadowing effects), $1/450$ m^{-1} (Delft3D domain) and $1/50$ m^{-1} (area of interest).

Sediment transport within the flow domains was calculated using the Van Rijn et al. (2004) transport equations with the suspended and bedload transport computed independently. Hereafter, the sum of both types is referred to as sediment transport. This sediment transport formula was chosen because it incorporates both currents and waves and resulted in a steady littoral drift (see Section 2.4). A single sediment fraction with a d_{50} of 250 μm was used in all domains, because it is optimal for shoal formation and migration (Herrling and Winter 2018). Bed level changes were calculated from gradients in sediment transport and sediment settling/entrainment using a morphological acceleration factor $M = 20$ to reduce computation time (Roelvink, 2006). Sensitivity analysis showed that the final results were unaffected by this value. The hydrodynamic boundary conditions consisted of semi-diurnal tides (amplitude 1 m and period 12 h) propagating along the coast and waves coming from the northwest (origin 335^o clockwise with respect to the north). The significant wave height and peak period for all model runs were 2.0 m and 7.5 s, respectively. These settings were motivated by the obtained tidal prism and littoral drift values, which are suitable for modeling cyclic behavior (Lenstra et al., 2019b).

2.2. Model simulations

The model runs presented in this study include both undisturbed reference model simulations and disturbed simulations with basin size reductions or relative sea-level rise. An overview of all simulations is shown in Table 1; the initial bathymetries are shown in Fig. 2. The reference simulation *undis100* is the 1 m tidal amplitude and 2 m significant wave height model run as described in (Lenstra et al., 2019b, run 2). This model run has clear cyclic channel-shoal dynamics similar to the ebb-tidal delta breaching model of FitzGerald (1988). The modeled cyclic behavior has three characterizing phases, each with a distinct relative importance of tides and waves. During Phase 1, the channel rotates in the clockwise direction; the rotation rate scales with significant wave height and is relatively unaffected by tidal flow. Subsequently, the shoal grows in the downdrift direction during Phase 2. During this phase, wave-induced sediment concentrations are advected by a combined wave- and tide-induced mean flow. The sediment concentration is significantly reduced at the downdrift side of the ebb-tidal delta as this part is partly sheltered from incoming wave energy by the ebb-tidal delta platform. This causes the shoal to grow and migrate. During Phase 3, a new channel breaches the ebb-tidal delta. The formation of the new channel scales with (1) peak ebb-flow transporting the sediment and (2) wave height increasing the bed-shear stress and the sediment concentration. However, for large ratios between wave height and tidal flow, the channel rotation continues and the breach is

Table 1
Overview of conducted model runs. Basin area is relative to 9 km by 3.5 km in the alongshore and cross-shore direction, respectively.

Run	Basin area	sea-level rise	Initial bathymetry
undist100	100%	0	no ebb-tidal delta
undist90	90%	0	no ebb-tidal delta
undist80	80%	0	no ebb-tidal delta
undist70	70%	0	no ebb-tidal delta
undist50	50%	0	no ebb-tidal delta
dist100→90	90%	0	*undis100* after 3400 days
dist100→80	80%	0	*undis100* after 3400 days
dist100→70	70%	0	*undis100* after 3400 days
dist100→50	50%	0	*undis100* after 3400 days
slr50	100%	0.5 cm/yr	*undis100* after 3000 days
slr100	100%	1 cm/yr	*undis100* after 3000 days
slr150	100%	1.5 cm/yr	*undis100* after 3000 days
slr200	100%	2 cm/yr	*undis100* after 3000 days
slr100 + 100→70	70%	1 cm/yr	*undis100* after 3400 days

postponed.

The other undisturbed runs initially only differ in basin surface area, as indicated by the red lines in Fig. 2. The reference runs *undis90*, *undis80*, *undis70* and *undis50* have 90%, 80%, 70% and 50% of the 31.5 km^2 basin surface area from *undis100*, respectively. Amongst these runs, the width/length-ratio of the basin was kept constant; test runs show that only reducing the width or the length yielded similar cyclic behavior.

For the disturbed runs, the bathymetries obtained after 3000 (for relative sea-level rise) or 3400 modeled days (for basin size reduction) in *undis100* were used as a starting bathymetry. To test the effect of basin size reduction, part of the basin size area was instantaneous removed from the model domain after 3400 days, i.e., directly after the breaching phase of the cyclic behavior. Test runs with the basin area reduction after 3000 days (during the shoal growth phase) instead of 3400 days yielded similar results with respect to changes in cyclic behavior, time scale and adaptation. The basin area reduction was either 10% (*dist100→90*), 20% (*dist100→80*), 30% (*dist100→70*) or 50% (*dist100→50*). Their outcome was compared to the undisturbed runs; for example, *dist100→70* was compared to both *undis100* and *undis70*.

To study how cyclic behavior of ebb-tidal deltas is affected by rising mean sea level, model runs were conducted with constant rates of rising sea level, ranging from 0.5 to 2 cm/year with 0.5 cm/year increments. These rates were based on Vermeersen et al. (2018), who projected rates for relative sea-level rise in 2100 for the Dutch Wadden Sea ranging from 0.22 to 1.83 cm/year. We did not take into account an acceleration of relative sea-level rise. The typical time scales of the cyclic evolution in the model are in the order 3–5 years, representative for German Wadden Sea systems (Ridderinkhof et al., 2016b). During such a period no effects of acceleration are expected. These disturbed model runs, with rising subtidal water level after 3000 days, are denoted as *slr50*, *slr100*, *slr150* and *slr200* for a rise in mean sea level per century of 50 cm, 100 cm, 150 cm and 200 cm, respectively. Their outcomes were compared to the undisturbed run with equal basin area (*undis100*). Test runs showed that outcomes the main findings were not sensitive to the initial bathymetry, i.e. increasing the mean sea level after 3400 instead of 3000 days.

Moreover, one test run (*slr100 + 100→70*) has been included that combines both the basin area reduction (30%) and sea-level rise (1 cm/year). The outcome of this model run will be discussed in Section 4.

2.3. Model analysis

For each model run, we analyzed and compared the:

- time scale of the cyclic behavior. For this, the period between successive breaching events (T_{breach}) was used. The ebb-tidal delta was said to breach when a new channel splits the 3.5 m isobath into an updrift and a downdrift part;
- cross-sectional area of the inlet (*CSA*), taken at the cross-section *CSInlet* (Fig. 1). For the runs with rising mean sea level, the area below the subtidal water level was computed;
- the volume of the ebb-tidal delta (V_{ETD}), obtained by summation of the difference between the modeled and an no-inlet bathymetry, multiplied by the grid cell area. Following Dean and Walton (1975), the no-inlet bathymetry was constructed based on the cross-shore profile at both sides of the inlet (*CSUp* and *CSDown* in Fig. 1). Only the positive values were taken into account, i.e. channels were not considered to be negative volume. Furthermore, the barrier islands were removed from the analysis by neglecting values above mean sea level.
- the orientation of the main channel, defined as the angle between the last and first grid point of the path of the main channel path with respect to the north (positive in clockwise direction). This path was determined in the following, iterative way. Starting at the deepest grid cell in the inlet, the next point of the main channel was the deepest grid cell that was both within 100 m of the previous point and further seaward from the inlet than the previous point. The end of the channel was reached either when the deepest point was above the 3.5 m isobath or when this point was more than 2000 m from the start of the channel (as in Lenstra et al., 2019b);
- tidal prism (*P*), i.e. the volume of water entering and leaving the basin each tidal cycle computed at *CSInlet*;
- mean flow and semi-diurnal flow amplitude at all locations. For this, harmonic analysis was used;
- significant wave height (tidally-averaged) computed at all grid cells adjacent to *CSInlet*;
- cumulative sediment transport values through the inlet (*CSInlet*), i.e. net import/export;
- cumulative sediment transport along the updrift and downdrift coast (*CSUp* and *CSDown*);
- shoal growth rate (Δh_s), defined as the total deposition per time unit in the area that has deposition exceeding 0.015 m/day (as in Lenstra et al., 2019b);
- breaching rate (Δh_b), defined as the average erosion per time unit in the part of the ebb-tidal delta that (1) is shallower than 3.5 m and (2) has erosion exceeding 0.006 m/day;

As discussed in Lenstra et al. (2019b), the volume of the ebb-tidal delta greatly depends on the no-inlet bathymetry. In that study, the no-inlet bathymetry was reconstructed after each tidal cycle because it better represented the formation and attachment of each shoals. Here, this procedure would lead to different no-inlet bathymetries for the different runs, which complicates the comparison between the undisturbed and disturbed runs. Therefore, here we opted for a fixed no-inlet bathymetry based on the 3400 days starting bathymetry (Fig. 2). Alternative fixed no-inlet bathymetries yielded similar results.

2.4. Model calibration and validation

Validation of the present model setup is needed to ensure that it is applicable to future scenarios and consistent with known empirical relationships. Firstly, calibration of the model was performed based on the stability of the tidal prism, the littoral drift and the cross-shore coastal profile. A major constraint in this calibration was a steady littoral drift, which was found to be necessary for a successful modeling of the dynamic equilibrium of cyclic behavior. Numerous test runs showed unrealistic shoreface steepening and coastal expansion, which caused the littoral drift to decrease in time. As a result, no morphodynamic equilibrium was obtained in these runs. Therefore, in order to reduce this shoreface steepening, the wave-related bed load transport factor *BedW* was set to a constant value of 0.3. This parameter setting kept the littoral drift and the position of the coastline relatively steady at the time scales of interest. However, all model runs still feature some limited shoreface steepening. Eventually, these changes in the cross-shore balance also affect the alongshore balance and changes in littoral drift are expected due to the shoreface steepening. Therefore, model runs were analyzed for the period that the littoral drift was steady, i.e., for most runs until roughly 8000 modeled days. Within this modeled period the littoral drift was unaffected by the changes in basin area and by the rising mean sea level. However, test runs with sea-level rise exceeding 2 cm/yr did show a steadily reducing littoral drift, which was why they were not included in this paper.

Secondly, empirical relationships between tidal prism, volume of the ebb-tidal delta and cross-section of the inlet were used for validation of the model. O'Brien (1931, 1969) identified a relationship between the cross-sectional area of an inlet (*CSA*) and the tidal prism (*P*) for systems in morphodynamic equilibrium. This so-called PA-relationship states $CSA = c \cdot P^n$ with c and n as correlation coefficients. Here, we adopted the methodology of Nahon et al. (2012), who showed that idealized model simulations can abide by this relationship with (c,n)-values similar to those of the observations of Jarrett (1976), covering 96 inlets with no or one jetties on the coastline of the USA. Similarly, we determined the (c,

n)-values based on all model simulations and compared the obtained values to those found by Nahon et al. (2012) and Jarrett (1976). For the undisturbed runs, P and CSA were averaged over the first two cycles of the model run, because they depend on the phase of the cyclic behavior. Because a basin reduction forces the system initially out of equilibrium (as will be shown in Section 3.2) and because rising mean sea level forces changes in P and CSA, for the disturbed runs P and CSA were averaged over the last two modeled cycles of cyclic channel-shoal dynamic (before the end of the run around 8000 modeled days). This analysis yields $c = 1.8{\cdot}10^{-5}$ and $n = 1.08$; this is in fair agreement with $c = 3.8{\cdot}10^{-5}$, $n = 1.03$ (Jarrett, 1976) and $c = 9.1{\cdot}10^{-5}$, $n = 1.00$ (Nahon et al., 2012) The factor 5 difference in c can be explained by the slightly different values of n and the fact we did not have a wide range in values of P. For typical values of $P \sim 10^7$ m^3, the model yields very similar values of CSA. Also, model results compare well with their observation: all but one (P, CSA)-points fall within the 95% confidence interval, thereby providing additional credibility to the model setup and its predictions. Only for a sea-level rise of 2 cm/year does the modeled behavior not abide the PA-relationship; the reason for this will be discussed in Section 3.3.

A similar empirical relationship between the tidal prism (P) and the volume of the ebb-tidal delta (V_{ETD}) was determined by Walton and Adams (1976): $V_{ETD} = a{\cdot}P^b$ with correlation coefficients a and b. Based on observations of 44 tidal inlets, they determined $a = 8.7 - 13.8{\cdot}10^{-5}$ and $b = 1.08 - 1.24$ (depending on the exposure of the inlets) with P in cubic feet and V_{ETD} in cubic yards. Analysis of the present model runs yields $a = 7.7{\cdot}10^{-5}$ ($a = 4.7{\cdot}10^{-3}$ when cubic meters were used) and $b = 1.23$. Furthermore, as extensively discussed in Lenstra et al. (2019b), the model also abides by the relationship between the ratio of tidal prism over littoral drift and type of cyclic behavior (Bruun and Gerritsen, 1960) and mimics the conceptual models of FitzGerald (1988). Overall, the modeling setup performs satisfactory, both for undisturbed model runs and for future scenarios.

3. Results

3.1. Undisturbed model runs

In each undisturbed run, several repeating cycles of channel rotation and breaching, development of a shoal and its subsequent migration and attachment to the downdrift island were modeled. Table 2 shows the time scales (T_{breach}), tidal prism (P), ebb-tidal delta volume (V_{ETD}) and cross-sectional area (CSA) for each simulation. Note that the parameters P, V_{ETD} and CSA were averaged over the first two cycles of the model run, because they depend on the phase of the cyclic behavior.

Even though the undisturbed runs yield a type of cyclic behavior similar to each other, several differences arise. Firstly, as can be seen from the average periods ($\overline{T_{breach}}$), smaller basins have shorter time scales. Secondly, Table 2 indicates that the volume of the ebb-tidal delta and the cross-sectional area of the inlet also depend on the basin surface area. This is because they both scale with tidal prism.

Table 2
Overview of model output for undisturbed runs with periods between successive breaches (T_{breach}) and its average value ($\overline{T_{breach}}$). The values for P (tidal prism), V_{ETD} (ebb-tidal delta volume) and CSA (cross-sectional area) are averaged over the first two cycles of cyclic behavior.

Run	T_{breach} (days)	$\overline{T_{breach}}$ (days)	P (Mm^3)	V_{ETD} (Mm^3)	CSA (m^2)
undist100	760, 1160, 1700, 1500, 1350	1294	55	11	4000
undist90	1010, 850, 1050	970	50	10.5	3600
undist80	1000, 1100, 700, 500, 700	800	45	9.7	3300
undist70	350, 750, 350, 750, 800, 950	658	38	9	2800
undist50	350, 400, 650, 450	463	30	7.5	2000

3.2. Reduced basin area

The simulations with reduced basin area are characterized by an adaptation period and a period with new cyclic behavior. During the adaptation period, there is significant change in the modeled magnitudes of mean and semi-diurnal flow in the inlet (shown in Fig. 3). These time-dependent values are the maximum value across the tidal inlet. Both values are initially but temporarily lowered by the reduction in basin area and tidal prism (Table 3), especially the semi-diurnal flow velocities. The effect of the smaller flow velocities in the inlet on the balance between sediment deposition by wave-driven littoral drift and sediment erosion by tidal currents (diagram of Escoffier, 1940) can be seen in Fig. 4a: in response to smaller flow velocities in the inlet, its cross-sectional area gradually becomes smaller. A new equilibrium is obtained, which brings the semi-diurnal flow velocities close to their original values (Fig. 3a). Table 3 shows that the corresponding values for tidal prism are roughly equal to those in the undisturbed run with equal basin area in Table 2 (e.g. *dist100→70* and *undis70*).

An adjustment time scale T was determined from the exponential fit of the cross-sectional area of the inlet as $CSA(t) = CSA_{new} + (CSA_{old} - CSA_{new}){\cdot}exp(-t/T)$ with t the number of modeled days since the basin reduction. For a 50% basin size reduction, the adjustment time scale is 1296 days. For 10%, 20% and 30% basin area reduction, T is 185, 343 and 772 days, corresponding roughly to 14%, 26%, and 60% of the typical time scale of undisturbed cyclic behavior (*undist100*), respectively. This means that the period of adjustment increases with increasing basin reduction.

The modeled ebb-tidal delta volumes are shown in Fig. 4b. It can be seen that a larger reduction in basin area causes a larger relative decline in volume. However, even though the inlet cross-sectional area and the tidal prism eventually converge to the value of the undisturbed runs with equal basin area, this is not the case for the volume (see difference between *undist80* and *dist100→80*). This can partly be explained by the fact there is no equilibrium volume yet in most model runs (see increasing trend for *undist100*). However, comparing the *dist100→50* and *undist50* simulations suggests this is not the only explanations. Both simulations have a steady ebb-tidal delta volume after 5000 days, but still have difference of roughly 0.5 Mm^3 in sediment volume. This shows that the ebb-tidal delta can keep part of its initial volume and have a larger volume than would be expected based on empirical relationships.

The changes in ebb-tidal delta also affect the wave energy that reaches the inlet and back-barrier basin. The smaller ebb-tidal deltas cause a decrease in both the width-averaged and the maximum significant wave height in the inlet (Fig. 4d, solid and dashed lines, respectively). The wave height in the inlet largely depends on the size of the updrift oriented secondary channel. Because this channel is both shallower and narrower for smaller basins, more wave energy dissipates seaward of the inlet. The decrease in size of the secondary channel for decreasing basin area is visible from the black depth contours in Figs. 8 and 9 and also affects the cross-sectional area (Fig. 4a).

Fig. 4e shows the additional cumulative sediment import caused by the basin size reduction. This is the difference in net sediment import between disturbed runs and *undist100*. Additional sedimentation of the basins for a 10–30% basin size reduction shows that the channels in the basin and the inlet are too big for the reduced basin. The additional cumulative import after 6200 days equates to an average sedimentation of the basin of 1.8 cm for *dist100→90*, 3.2 cm for *dist100→80* and 3.7 cm for *dist100→70*. After the initial adjustment period, no additional sediment import is modeled. During the adjustment period the inlet and basin find a new dynamic equilibrium, as further illustrated by the balance between tidal flow and inlet cross-sectional area (Figs. 3 and 4a, respectively); it can be seen that the inlet converges to the dynamic equilibrium in the reference run with equal basin size.

Surprisingly, for a 50% basin area reduction (*dist100→50*), less

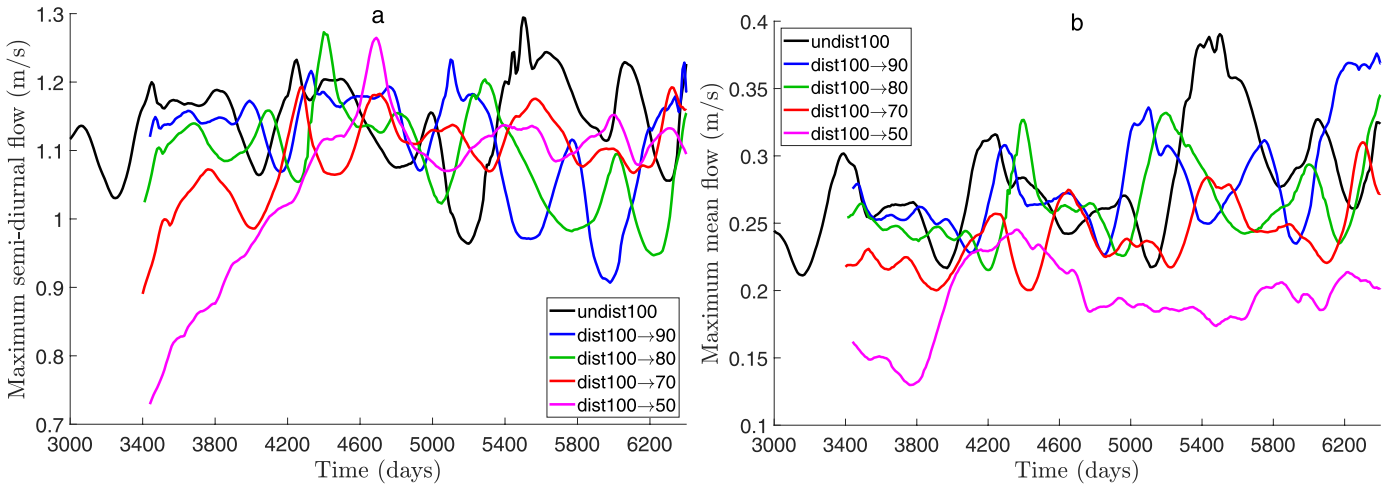

Fig. 3. For undist100 and the reduced basin runs the maximum value in the inlet of the (a) semi-diurnal flow amplitude and (b) mean flow magnitude.

Table 3
Period between successive breaches for the disturbed runs with a reduction in basin area after 3400 days with T_{first} the period of the first cycle and T_{breach} all subsequent periods. Here, $\overline{T_{breach}}$ is the average period after first cycle and P the tidal prism averaged over the first two cycles of cyclic behavior.

Run	T_{first} (days)	T_{breach} (days)	$\overline{T_{breach}}$ (days)	P (Mm^3)
dist100→90	860	850, 1050, 1050	983	50
dist100→80	960	800, 1250	1025	46
dist100→70	1260	750, 900, 750	800	38
dist100→50	860	850, 300, 400, 400, 350, 550, 600, 500, 800	528	32

infilling is modeled. In this case, only after the cross-sectional area has adjusted to the reduced tidal prism, more sediment is imported than in *undist100*. Here, the average sedimentation in the basin after 6200 days is only 1.3 cm. Possibly, the weaker mean flow magnitudes (Fig. 3b) limit the capacity of the tidal flow to import sediment.

Fig. 4f shows the additional cumulative sediment transport along the downdrift coast forced by the basin size reduction. The corresponding change in cumulative sediment transport along the updrift coast (roughly 0.9 Mm^3/year) is less than 0.01 Mm^3/year. Another difference between *dist100→50* and the other model runs can be seen. For a 50% basin size reduction, the sediment transported along the downdrift coast is persistently lower than for the undisturbed model runs and the model runs with a 10–30% basin size reduction. However, the difference is much smaller than the absolute littoral drift magnitude.

Basin area reductions also impact the cyclic behavior of the ebb-tidal delta. Table 3 shows that the effect of the basin reduction on the periods between successive breaches during and after the adjustment period differs. Note that there is considerable variability of T_{breach} within each model run (both for undisturbed and disturbed model runs). However, relating the periods in the disturbed runs to those in the reference runs, does consistently show the following two effects. Firstly, the cyclic channel-shoal dynamics are initially slowed down by the reduction in basin size area and tidal prism. Within each disturbed model run, the duration of the first cycle (T_{first}) exceeds that of *undist100*: for the disturbed runs, T_{first} is between 860 and 1260 days, whereas the matching period in *undist100* is 760 days. Secondly, the subsequent periods (T_{breach}) are consistently shorter than in the undisturbed model run. This apparent acceleration is unsurprising as the undisturbed runs showed that period between breaches correlates with basin area and tidal prism (Table 2). The physical mechanisms leading to the initial longer and the eventual shorter periods of the cyclic behavior will be discussed in Section 4.1. The average values $\overline{T_{breach}}$ suggest shows that the time scale remains longer than that of the undisturbed run with equal basin area, regardless of the basin area reduction. This suggests that the eventual acceleration after basin area reduction is limited such that the eventual period of cyclic behavior is longer than what would be expected based on the tidal prism. However, as can be seen in Tables 2 and 3, the modeled period varies greatly within all model runs, which could also explain the longer period.

3.3. Relative sea-level rise

For the runs with different rates of relative sea-level rise, the bathymetries are initially very similar; but eventually, as the mean water level further rises, the cyclic behavior continues with noticeable changes. The period between successive breaches, listed in Table 4, shortens with rising mean sea level for the lower rates ($\leq$ 1.5 cm/yr: *slr50*, *slr100* and *slr150*). Fig. 6c shows that the shorter periods are concurrent with an increase in the minimum channel orientation. Breaches that are followed by a more downdrift oriented new channel (larger minimum channel orientation) are also followed by shorter period. This downdrift shift is concurrent with slightly smaller semi-diurnal flow velocities (Fig. 5a), which can be explained by an increase in inlet cross-sectional area (Fig. 6a). For the lower rates of sea-level rises, the larger minimum channel orientation explains the shorter third and fourth period.

Only when the relative sea-level rise is 2 cm/yr (*slr200*), the cyclic behavior slows down. The larger periods are related to an increase in cross-sectional area larger than that for the lower rates of sea-level rise. The increase in cross-sectional area is particularly evident after 5500 days. This increase has the effect of significantly smaller flow velocities (orange line in Fig. 5a), which in turn causes breach postponement. In contrast to the lower rates of rising sea level, reduced tidal flow causes longer periods between successive breaching events. Again, the time scale is linked to the channel orientation after the breach (Fig. 6c); in this case, the new channel has a more updrift orientation. Based on this transition from shorter to longer periods, we conclude that there is a critical rate of relative sea-level rise for cyclic behavior, in this system between 1.5 and 2 cm/yr. Above the critical rate, the increase in cross-sectional area cannot be compensated by additional sediment input from the littoral drift, slowing down the cyclic evolution of the ebb-tidal delta. Below the critical rate, the cross-sectional area of the inlet is relatively steady and shorter periods were modeled.

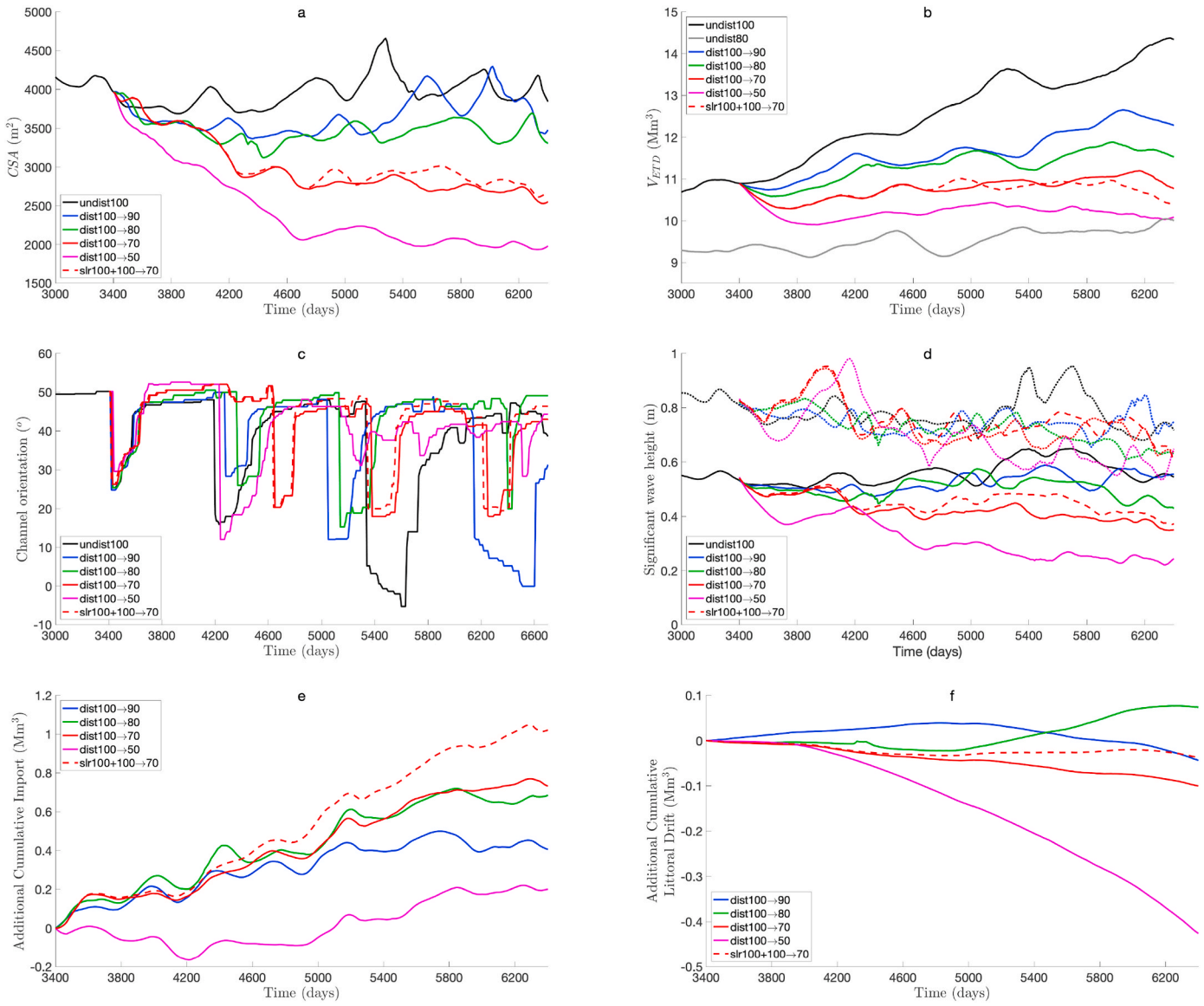

Fig. 4. For the reduced basin runs (a) cross-sectional area of the inlet, (b) volume of the ebb-tidal delta, (c) the orientation of the main channel, (d) the average (solid lines) and maximum (dotted) significant wave height in the inlet, (e) additional cumulative sediment import, and (f) additional cumulative littoral drift along the downdrift coast.

Table 4
Period between successive breaches for the disturbed runs with rising subtidal water level together with undist100 for reference. Only the first 4 periods are shown.

Run	T_{breach} (days)
undist100	760, 1160, 1700, 1500
slr50	760, 1130, 1430, 1480
slr100	760, 1110, 1450, 1200
slr150	760, 1220, 1350, 1170
slr200	760, 1150, 1860, 1960

Fig. 6b shows the relative volume of the ebb-tidal delta, i.e., the difference between the volumes in the runs with and without relative sea-level rise. The solid lines are based on the initial mean water level, whereas for the dashed lines the volume is corrected for relative sea-level rise. Surprisingly, the ebb-tidal deltas maintain most of their volume; as the dashed lines show, they are simply further submerged because the water level rises. As expected, the increased water depth reduces the offshore wave energy dissipation and thus increases the wave height in the inlet (Fig. 6d).

Fig. 6e and f shows the additional sediment transport through cross-sections across the inlet and perpendicular to the downdrift coast, respectively. The former shows that more sediment is imported than in *undis100*. For relative sea-level rise below the critical rate, the additionally imported sediment scales with increasing rate of sea-level rise. The additional cumulative import until 7000 days equates to an average sedimentation of the basin of roughly 0.15 cm/yr for *slr50*, 0.17 cm/yr for *slr100* and 0.32 cm/yr for *slr150*. In contrast, for *slr200*, eventually no more sediment is imported than for *slr150*. This suggests that the declining peak flow velocities due to the oversized cross-sectional area limit the capacity of tidal currents to transport sediment into the basin. The sediment flux along the downdrift coast (Fig. 6f) reveals another difference between the model runs with rate of relative sea-level rise below and above the critical value. For rates of relative sea-level rise below the critical rate, the littoral drift at the downdrift coast increases, possibly because of the shorter periods of cyclic behavior. However, for 2 cm/yr relative sea-level rise, a decrease in littoral drift is modeled at the downdrift island. The change in cumulative sediment transport

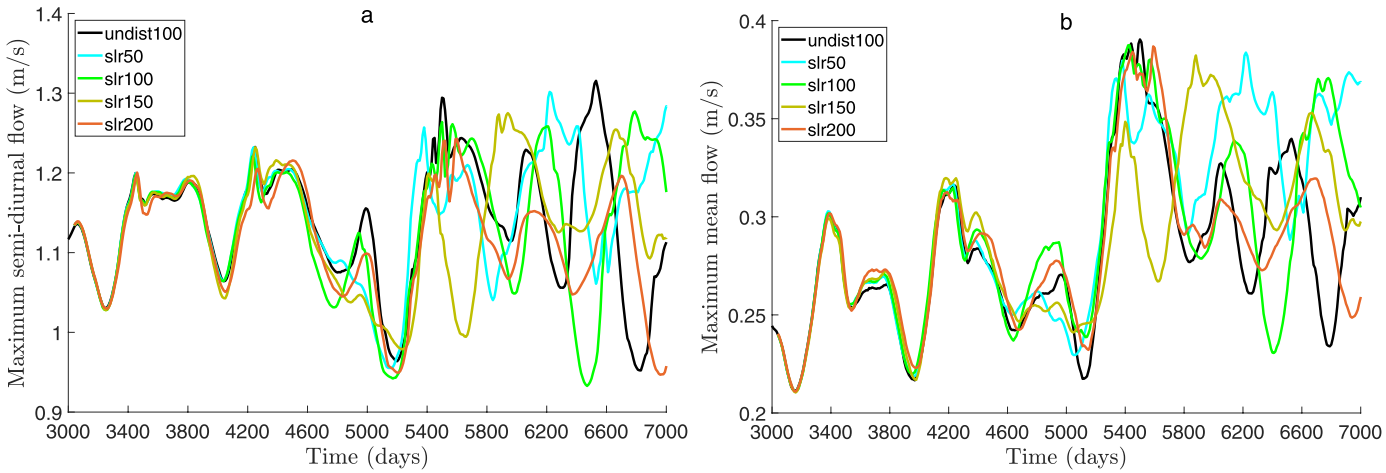

Fig. 5. For undist100 and the runs with relative sea-level rise the maximum tidal flows amplitudes in the inlet with (a) semi-diurnal flow and (b) mean flow.

along the updrift coast due to sea-level rise is negligible (less than 0.02 Mm^3).

4. Discussion

Deflecting channels and periodic breaching are natural sediment bypassing mechanisms at many ebb-tidal deltas (FitzGerald, 1988; FitzGerald et al., 2000; Ridderinkhof et al., 2016b). The feedbacks between this cyclic behavior and the underlying physical processes are relatively well understood (Cayocca, 2001; Bertin et al., 2009; Ridderinkhof et al., 2016a; Lenstra et al., 2019a, b). Some tidal basins have been reduced in area in the last century, disrupting the natural dynamics (FitzGerald et al., 1984; Van de Kreeke, 2006; Elias et al., 2012). Many tidal inlet systems are further affected by relative sea-level rise (Van der Spek, 2018; Vermeersen et al., 2018; Wang et al., 2018). Observations indicate that these anthropogenic influences resulted in erosion of ebb-tidal deltas; slowing down of cyclic behavior of ebb-tidal deltas; and additional sediment import into the basin. These patterns were reproduced by the model. Furthermore, we have quantified the different effects and differentiated between relative sea-level rise and changes in basin area. In the discussion we will analyze why ebb-tidal delta dynamics change (Section 4.1) and put our results in a broader perspective (Section 4.2).

4.1. Physical mechanisms

We have reproduced the observations that a reduction in basin area causes initially longer and eventually shorter cycle periods and we have discussed the underlying mechanisms. The patterns of erosion/deposition, mean and semi-diurnal flow velocities and (tidally-averaged) sediment transport were analyzed during the three phases of cyclic behavior to explain the longer duration of the first cycle. Fig. 7 shows these parameters after 3400 days, i.e., directly after model restart and during the phase of channel rotation. At this moment, the morphology is the same for all model runs such that the instantaneous effect of basin reduction on tidal currents and sediment dynamics was isolated. The green contour indicates the change in tidal flow magnitude, particularly in the inlet (as in Fig. 3a) and in the main channel. The results show that the deepening of the new channel (blue) scales with basin area. The maximum erosion along the black line across the channel is 0.033 m/day for *undist100* and 0.029, 0.025, 0.020 and 0.014 m/day for a 10%, 20%, 30% and 50% basin reduction, respectively. Furthermore, also the deposition in the seaward part of the delta slows down for larger reduction in basin area. However, the maximum deposition rate along the black line in the area flanking the channel is, with values ranging between 0.1055 and 0.1077 m/day, surprisingly similar. This is because the wave-induced patterns of mean flow (yellow/black vectors) and sediment transport (white/magenta) over the shallow ebb-tidal delta platform are relatively unaffected. Based on the similar deposition rates, it is concluded that the longer duration of the first cycle cannot be explained by changes in the channel rotation rate. This is supported by the fact that the channel orientations after 3600 days are roughly equal (see Fig. 4c). However, due to the reduced tidal flow, both the size of the channel and growth of the ebb-tidal delta are reduced.

Fig. 8 shows the patterns of erosion/deposition, mean and semi-diurnal flow velocities and (tidally-averaged) sediment transport after 3800 days. At this moment, all model runs are characterized by shoal growth, as indicated by the areas of deposition on the downdrift side of the ebb-tidal delta. The shoal growth was quantified by the shoal growth rate, i.e., total deposition in the area in thick black contour in Fig. 8. For *undist100*, the shoal growth rate is 10229 m^3/day, whereas for the runs with basin reduction this is 7837 m^3/day (*dist100→90*), 6338 m^3/day (*dist100→80*), 5909 m^3/day (*dist100→70*) and 4098 m^3/day (*dist100→50*). As shown in Lenstra et al. (2019b), the shoal growth scales both with wave-induced sediment concentration and with mean flow magnitude (both tide- and wave-induced) over the ebb-tidal delta platform. Here, there is no significant variations in sediment concentration on the ebb-tidal delta platform amongst the simulations with different basin sizes, whereas comparison of the black/yellow vectors indeed show that the mean flows during the first cycle decrease with basin area. Therefore, we conclude that the dampened shoal growth due to a drop in mean flow at least partly explains the longer duration of the first cycle.

After the phase of shoal growth, the breaching of the ebb-tidal delta is initiated. The breaching rate was calculated as the average erosion in the area in thick black contour in Fig. 9. This figure shows the patterns of erosion/deposition, mean and semi-diurnal flow velocities and (tidally-averaged) sediment transport when the breaching rate is maximum in the first cycle. For a 10% or 20% basin reduction, the breaching rates (0.0148 m/day and 0.0153 m/day, respectively) are significantly higher than that in the reference run (0.0115 m/day). This increase in erosion is due to a $\sim$ 10% increase in sediment concentration. For a 30% basin reduction, the breaching rate of 0.0117 m/day in the first cycle is close to that of the reference run. Only for a 50% basin reduction is a lower breaching rate obtained for the first breach (0.0086 m/day). Here, both the sediment concentration and the mean peak ebb flow velocity are roughly $\sim$ 10% lower than in the reference run. This suggests that the adaptation is completed for *dist100→90* and *dist100→80*, almost completed for *dist100→70* and continues for *dist100→50*.

The shoal growth rate and the breaching rates for all reference runs and runs with basin reduction are summarized in Table 5. A distinction is made between the rates before and after the adjustment. During the

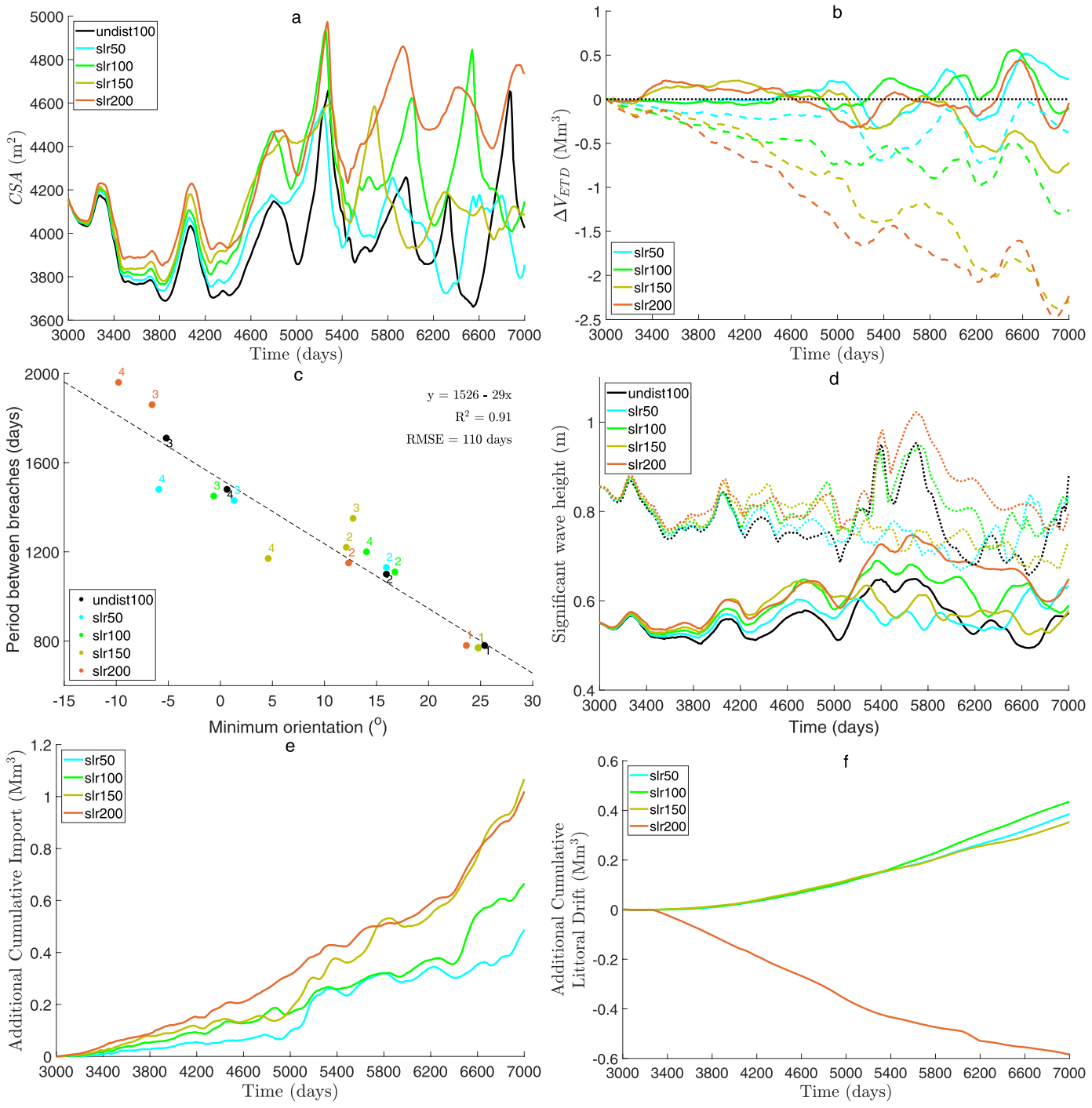

Fig. 6. For the runs with relative sea-level rise (a) cross-sectional area of the inlet, (b) relative volume of the ebb-tidal delta (solid lines: based on the initial mean water level; dashed lines: based on the actual mean water level), (c) the minimum orientation after the breach versus the period between the two breaches, (d) the average (solid lines) and maximum (dotted) significant wave height in the inlet, and (e) additional cumulative sediment import, and (f) additional cumulative littoral drift along the downdrift coast.

adjustment period, the shoal growth rate decreases with decreasing basin size, whereas the opposite effect is found after the adjustment period. Following the reference runs, the shoal growth rate increases with decreasing basin size. A similar trend is found for the breaching rate: the breaching rates correlates positively and negatively with basin size before and after the adjustment period, respectively. For *dist100→90* and *dist100→80*, the values in Fig. 9 are similar to those in the subsequent cycles, indicating that the adaptation was completed. This is not the case for *dist100→70* and *dist100→50*; this slower adaptation corresponds with the longer adaptation period and the largest values for T_{first}.

In conclusion, the initial slowing down of the cyclic behavior can be attributed to an initial dampening of the shoal growth phase, whereas the channel rotation phase is unaffected. The subsequent acceleration is in turn due to an increase in shoal growth rate and breaching rate after the adjustment period. It remains unclear why T_{first} of *dist100→70* exceeds that of *dist100→50*, despite the lower shoal growth and breaching rates for the latter. Possibly, this is due to the smaller ebb-tidal delta.

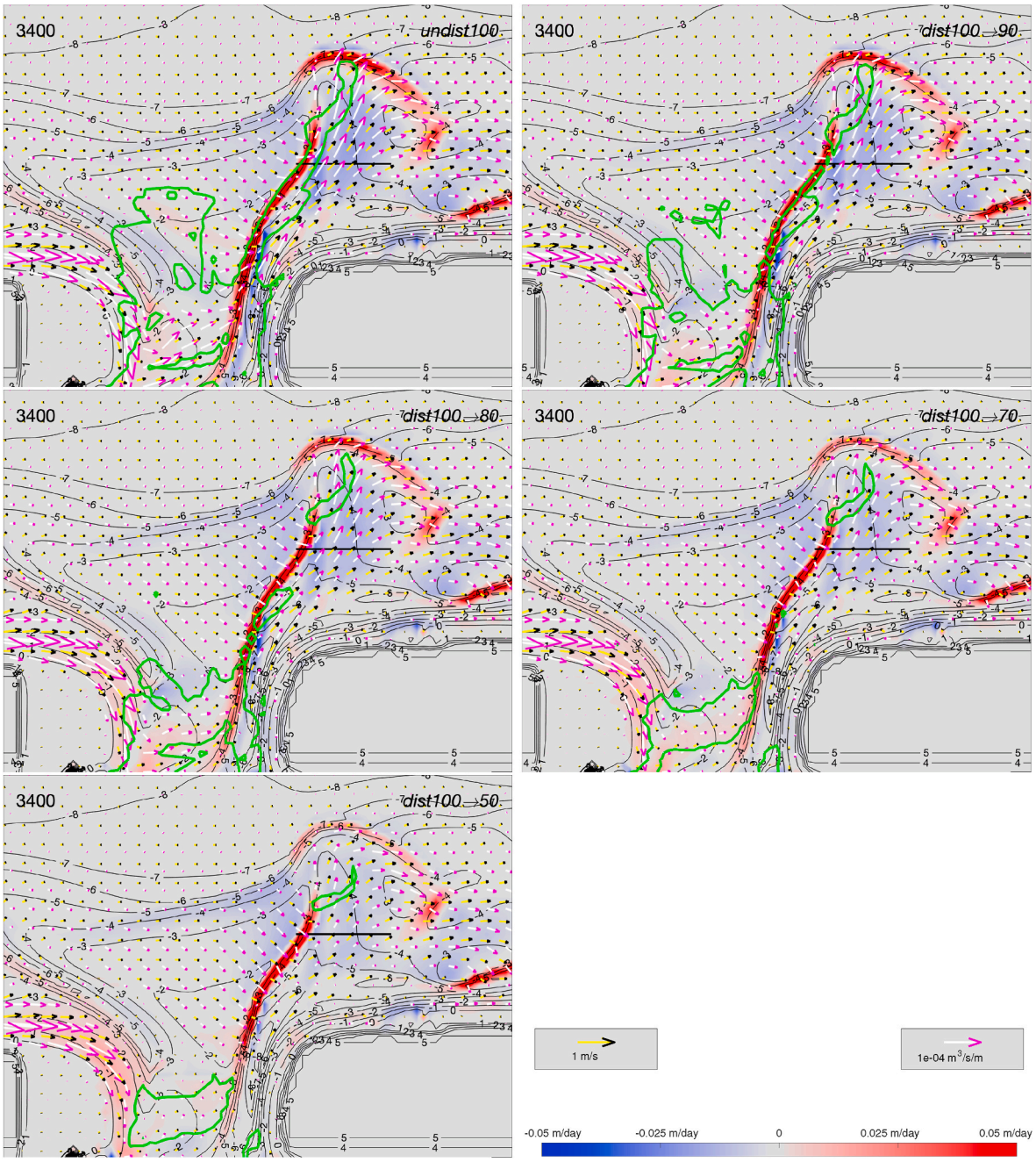

Fig. 7. Erosion (blue) and deposition (red) after 3400 modeled days. The vectors represent tidally-averaged total sediment transport (white/magenta) and flow velocities (yellow/black). The vectors are shown in every third grid cell in both directions. The green line encloses the area with semi-diurnal flow magnitude exceeding 0.23 m/s. The shown area is 4 km (east-west direction) by 3 km (north-south). In the upper right corner of each panel, the model run is shown. (For interpretation of the references to color in this figure legend, the reader is referred to the Web version of this article.)

4.2. Comparison and shortcomings

This study focused on relatively short basins with a standing tidal wave, such as the Frisian Inlet. Our results explain what has happened at this inlet, where the closure of the Lauwerszee caused additional import of sediment and slowed down the first cycle of channel-shoal dynamics (Biegel and Hoekstra, 1995; Oost, 1995; Van de Kreeke, 2006). We found that the adjustment time scale increases with basin area reduction. Note that the observed formation of an exceptionally large shoal at the Frisian Inlet (Elias et al., 2012) was not reproduced in the present study. The modeled drop in ebb-tidal delta volume was also observed at other inlets which had a reduction in basin area, such as the San Francisco Bay (Dallas and Barnard, 2011). Furthermore, our results indicate that in the future (after the adjustment) the morphological development of the Frisian Inlet and similar inlets will accelerate with shorter period of cyclic behavior because of faster shoal growth and breaching of the ebb-tidal delta. The shorter time scale of the cyclic behavior matches the observations of Gaudiano and Kana (2001) and Ridderinkhof et al. (2016b), who found that the period of the cyclic behavior correlates positively with the tidal prism. It appears that the typical period after the adjustment remains longer than the typical period in the undisturbed runs with equal basin area. Similarly, the volume of the ebb-tidal delta after the adjustment was lower than in *undis100*, but exceeded that of the undisturbed runs with equal basin area. Because larger ebb-tidal deltas tend to have a longer period between successive breaches/shoal attachments, it is likely that the latter two results are interrelated.

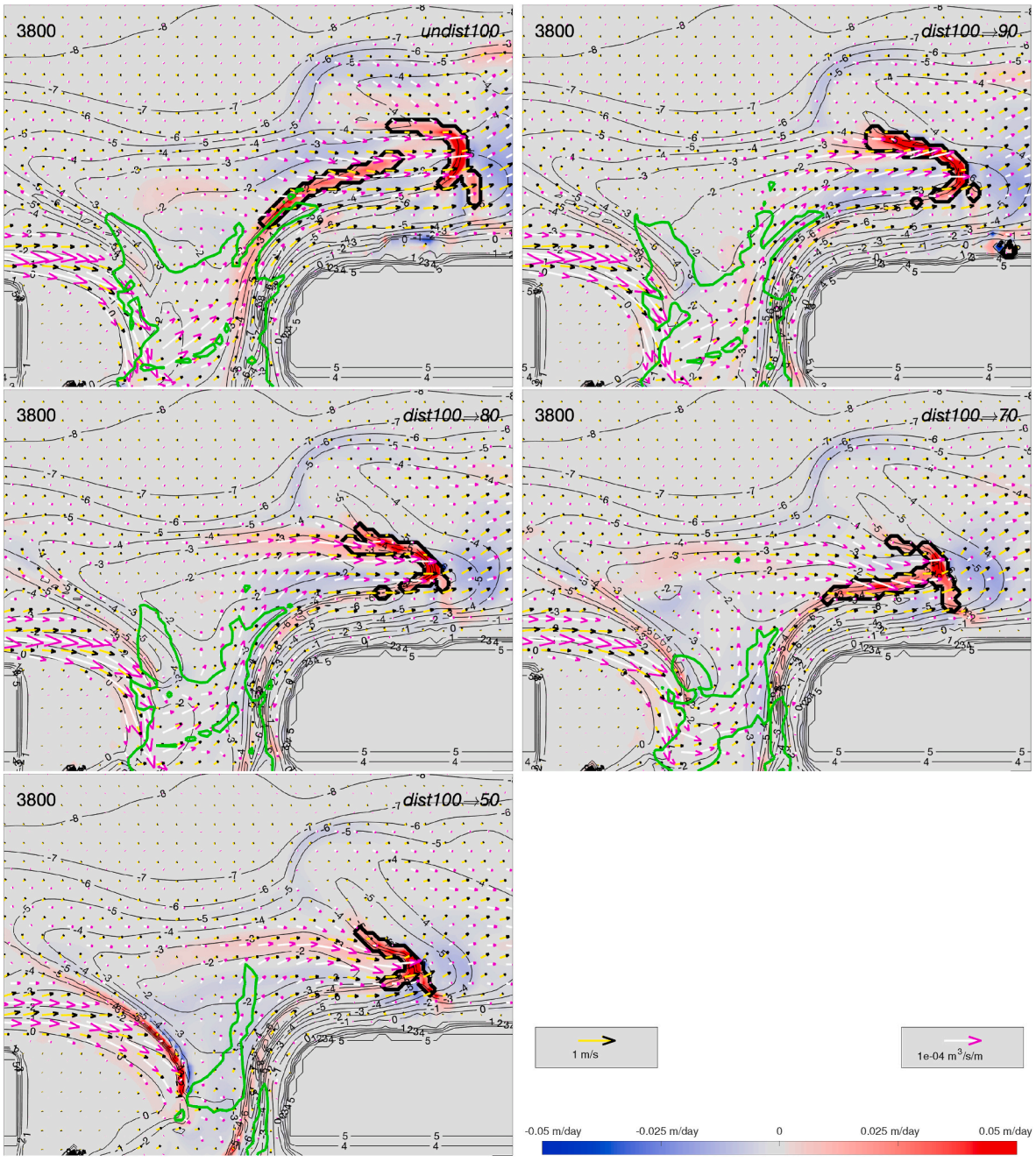

Fig. 8. As Fig. 7, but after 3800 modeled days.

Furthermore, the wave height in the inlet decreased with basin area because of the also decreasing size of the secondary (updrift oriented) channel, which is between the inlet and the predominant wave direction. This reduction is contrary to Lenstra et al. (2019a), where the Ameland Inlet was best protected from incoming waves when the main channel has an updrift orientation. In that case, more energy dissipated on the ebb-shield and the shallow areas flanking this channel, whereas in this study, the dissipation on these shallow areas was similar amongst the runs. This discrepancy might be explained by the spatial dimensions (Ameland Inlet is one order of magnitude larger than the idealized inlet in the present study) and by the orientation of the main channel (updrift/shore-normal for Ameland, downdrift/shore-normal here).

In some systems, reduction of the basin area has lead to an increase in tidal prism. For example, at the Texel and Vlie basins in the Dutch Wadden Sea, the construction of the Afsluitdijk caused the shift from a propagating to a standing tidal wave (Ridderinkhof et al., 2014). Resonance effects subsequently increased the tidal prism. However, the effect of such a transition is beyond the scope of this study.

In our simulations, the volumes of the ebb-tidal deltas subject to relative sea-level rise were relatively unaffected. They were simply submerged further because of the rising subtidal water levels. This implies that the sediment that has been observed to be imported into the basin in times of sea-level rise (Becherer et al., 2018; Wang et al., 2018), originates not from the ebb-tidal delta, but from other areas. Also, this suggests that the observed historic erosion of Dutch ebb-tidal deltas (Elias et al., 2012) was primarily caused by the basin reduction and not by the relative sea-level rise. Nevertheless, when the average water depth above the ebb-tidal deltas increased, less offshore wave energy dissipation was modeled. Because, as a result, the wave height increased in the inlet and the basin, this will potentially cause erosion of intertidal

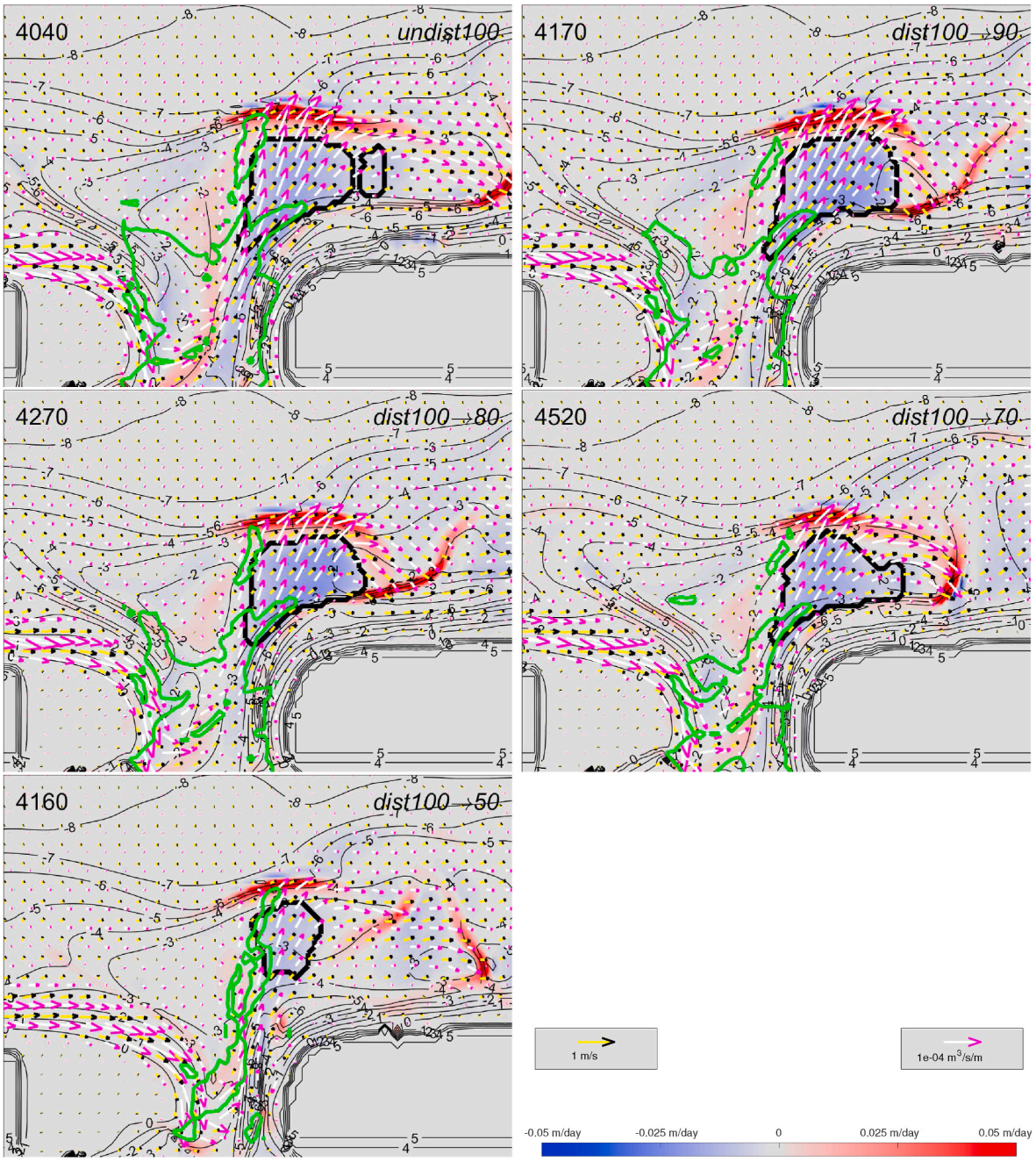

Fig. 9. As Fig. 7, but when the breaching rate is maximum during the first cycle.

flats in the basin. Furthermore, more energetic waves can propagate into the nearshore zone of the updrift tip of barrier islands, which further exposes the already eroding island heads.

In our model runs, the additional import of sediment was not sufficient to compensate for the accommodation space created in the basins. This is probably because of the relatively coarse sediment used in this study. It is known that finer sediment is transported more easily into the basin than coarse sediment (e.g. Sha, 1990; Gao and Collins, 1994; Herrling and Winter 2014; Zhou et al., 2015). However, it was not the objective of this study to examine or replicate the morphological response of the basin area, but that of the ebb-tidal delta. Wang et al. (2018) studied the effects of relative sea-level rise on sediment dynamics and morphology at the Dutch Wadden Sea and showed that each tidal basins has an individual critical rates for 'drowning' of intertidal flats. In other words, if the pace of rising mean sea level exceeds this rate, the maximum volume of imported sediment is no longer sufficient to maintain a portion of intertidal flats. Here, we found a similar critical rate of relative sea-level rise for cyclic behavior. Above this rate, the cross-section of the inlet was not in balance with the tidal flow, slowing down the cyclic channel-shoal dynamics. These longer periods between successive breaches were linked to an updrift shift in breach location. In contrast, if relative sea-level rise was below the critical rate, shorter period were associated with a downdrift shift in breach location.

This modeling study showed the connected adjustment of cyclic behavior, ebb-tidal delta volume, inlet cross-sectional area, tidal flow amplitudes and sediment import for both relative sea-level rise and basin area reduction. Many cyclic ebb-tidal deltas are located in an environment characterized by land reclamation, subsidence and/or sea-level rise. The outcomes of this study contribute to our understanding of the long-term evolution of tidal inlets in such an environment.

Table 5
The typical values for shoal growth rate (Δh_s) and the breaching rate (Δh_b) during and after the adjustment period.

Run	Δh_s (10^4 m^3/day) adjustment	Δh_s (10^4 m^3/day)	Δh_b (m/day) adjustment	Δh_b (m/day)
undist100	n.a.	0.9–1.1	n.a.	0.011–0.013
undist90	n.a.	1.0–1.3	n.a.	0.011–0.015
undist80	n.a.	1.0–1.7	n.a.	0.012–0.016
undist70	n.a.	1.4–1.6	n.a.	0.015–0.017
undist50	n.a.	1.3–1.7	n.a.	0.016–0.025
dist100→90	0.8	1.2–1.5	n.a.	0.012–0.015
dist100→80	0.7	1.2–1.7	n.a.	0.013–0.016
dist100→70	0.6	1.3–1.6	0.012	0.014–0.016
dist100→50	0.4	1.4–1.7	0.009	0.018–0.026

The focus of this paper is on the separate impacts of basin area reduction and relative sea-level rise. However, one model run has been conducted that combines the basin area reduction with relative sea-level rise (*slr100 + 100→70*). The outcome has been added to Fig. 4 (red dashed line). It can be seen that for the shown parameters, the combined effect is not very different from adding the effects of the two individual cases (*slr100* and *dist100→70*). For example, because both *slr100* and *dist100→70* feature additional sediment import, even more sediment is imported for *slr100 + 100→70*. Furthermore, the periods between successive breaches are 1250, 750, 880 and 700 days. Comparing those to *dist100→70* (Table 3) shows an acceleration due to the relative sea-level rise below the critical rate. It remains unknown whether the effects of relative sea-level rise and basin reduction dominate over one another and how this depends on the rate of relative sea-level rise and on the basin area.

5. Conclusions

This study has explored how natural cyclic behavior of ebb-tidal deltas and its time scale for short tidal basins are affected by an instantaneous reduction in basin area and by relative sea-level rise. To this aim, numerical model simulations were used which follow well-known empirical relationships. Back-barrier basin area reductions, which are common in many tidal inlet systems worldwide, lead to longer periods of cyclic behavior during an initial adjustment period and shorter periods after the adjustment. The initial longer periods were linked to severely reduced tidal flow in the inlet, an oversized cross-sectional area, dampened shoal growth and slower breaching of the ebb-tidal delta. Simultaneously a relative decrease in ebb-tidal delta volume and tidal prism was found. This decrease in tidal prism is eventually also related to the shorter periods of cyclic behavior after the adjustment period. Despite the erosion of ebb-tidal delta, the wave height in the inlet decreased because channels silted up.

We found shorter periods of cyclic channel-shoal dynamics for relative sea-level rise below a critical rate of 1.5 cm/yr. In this case, the sediment supplied to the inlet by the littoral drift compensated for the increase in cross-sectional area due to the rising water level. The acceleration of the cycle was related to a downdrift shift in breach location due to a small decrease in peak flow magnitudes. However, above the critical rate, significantly smaller flow velocities in the inlet caused the cyclic behavior to slow down. The ebb-tidal deltas maintained their volume, but because the water depth increased, so did the wave height in the inlet.

Declaration of competing interest

The authors declare that they have no known competing financial interests or personal relationships that could have appeared to influence the work reported in this paper.

Acknowledgments

We would like to thank B.G. Ruessink for critical reading. Furthermore, we thank the anonymous reviewers and the journal editors for their helpful suggestions. Funded by the Netherlands Organisation for Scientific Research (NWO) (project 869.15.009).

References

Battjes, J.A., Janssen, J.P.F.M., 1978. Energy loss and set-up due to breaking of random waves. In: Coastal Engineering 1978, pp. 569–587.
Becherer, J., Hofstede, J., Gräwe, U., Purkiani, K., Schulz, E., Burchard, H., 2018. The wadden sea in transition-consequences of sea level rise. Ocean Dynam. 68 (1), 131–151.
Beck, T.M., Kraus, N.C., 2011. New ebb-tidal delta at an old inlet, shark river inlet, New Jersey. J. Coast Res. 98–110.
Bertin, X., Fortunato, A.B., Oliveira, A., 2009. A modeling-based analysis of processes driving wave-dominated inlets. Continent. Shelf Res. 29 (5), 819–834.
Biegel, E., Hoekstra, P., 1995. Morphological response characteristics of the zoutkamperlaag, Frisian inlet (The Netherlands), to a sudden reduction in basin area. In: Tidal Signatures in Modern and Ancient Sediments, vol. 24, pp. 85–99 (Blackwell London).
Booij, N., Ris, R.C., Holthuijsen, L.H., 1999. A third-generation wave model for coastal regions: 1. model description and validation. J. Geophys. Res.: Oceans 104 (C4), 7649–7666.
Bruun, P., Gerritsen, F., 1960. Stability of coastal inlets. Coast. Eng. Proc. 1 (7), 23.
Cayocca, F., 2001. Long-term morphological modeling of a tidal inlet: the arcachon basin, France. Coast. Eng. 42 (2), 115–142.
Dallas, K.L., Barnard, P.L., 2011. Anthropogenic influences on shoreline and nearshore evolution in the san francisco bay coastal system. Estuar. Coast Shelf Sci. 92 (1), 195–204.
Dean, R.G., Walton, T.L., 1975. Sediment transport processes in the vicinity of inlets with special reference to sand trapping. Geol. Eng. 129–149.
Deltares, 2014. Simulation of Multi-dimensional Hydrodynamic Flows and Transport Phenomena, Including Sediments. User Manual Delft3D-FLOW. the Netherlands, p. 690.
Dissanayake, D.M.P.K., Roelvink, J.A., Van der Wegen, M., 2009. Modelled channel patterns in a schematized tidal inlet. Coast. Eng. 56 (11), 1069–1083.
Elias, E.P.L., Van der Spek, A.J.F., Wang, Z.B., De Ronde, J., 2012. Morphodynamic development and sediment budget of the Dutch wadden sea over the last century. Neth. J. Geosci. 91, 293–310, 03.
Escoffier, F.F., 1940. Hydraulics and stability of tidal inlets. Shore Beach 8, 114–115.
FitzGerald, D.M., 1982. Sediment bypassing at mixed energy tidal inlets. In: Coastal Engineering 1982. ASCE, pp. 1094–1118.
FitzGerald, D.M., 1988. Shoreline erosional-depositional processes associated with tidal inlets. In: Hydrodynamics and Sediment Dynamics of Tidal Inlets. Springer, pp. 186–225.
FitzGerald, D.M., Kraus, N.C., Hands, E.B., 2000. Natural Mechanisms of Sediment Bypassing at Tidal Inlets. Technical report, DTIC Document.
FitzGerald, D.M., Penland, S., Nummedal, D., 1984. Control of barrier island shape by inlet sediment bypassing: east Frisian islands, west Germany. Mar. Geol. 60 (1–4), 355–376.
Gao, S., Collins, M., 1994. Analysis of grain size trends, for defining sediment transport pathways in marine environments. J. Coast Res. 70–78.
Gaudiano, D.J., Kana, T.W., 2001. Shoal bypassing in mixed energy inlets: geomorphic variables and empirical predictions for nine South Carolina inlets. J. Coast Res. 280–291.
Hansen, J.E., Elias, E., Barnard, P.L., 2013. Changes in surfzone morphodynamics driven by multi-decadal contraction of a large ebb-tidal delta. Mar. Geol. 345, 221–234.
Herrling, G., Winter, C., 2014. Morphological and sedimentological response of a mixed-energy barrier island tidal inlet to storm and fair-weather conditions. Earth Surf. Dynam. 2 (1), 363–382.
Herrling, G., Winter, C., 2018. Tidal inlet sediment bypassing at mixed-energy barrier islands. Coast. Eng. 140, 342–354.
Holthuijsen, L.H., 2010. Waves in Oceanic and Coastal Waters. Cambridge University Press.
Jarrett, J.T., 1976. Tidal Prism-Inlet Area Relationships, vol. 3. US Department of Defense, Department of the Army, Corps of Engineers ?.
Komen, G.J., Hasselmann, K., Hasselmann, K., 1984. On the existence of a fully developed wind-sea spectrum. J. Phys. Oceanogr. 14 (8), 1271–1285.
Lenstra, K.J.H., Pluis, S.R.P.M., Ridderinkhof, W., Ruessink, G., van der Vegt, M., 2019a. Cyclic channel-shoal dynamics at the ameland inlet: the impact on waves, tides, and sediment transport. Ocean Dynam. 69.
Lenstra, K.J.H., Ridderinkhof, W., van der Vegt, M., 2019b. Unraveling the mechanisms that cause cyclic channel-shoal dynamics of ebb-tidal deltas: a numerical modeling study. J. Geophys. Res.: Earth Surf. 124.
Lesser, G.R., Roelvink, J.v., Van Kester, J., Stelling, G., 2004. Development and validation of a three-dimensional morphological model. Coast. Eng. 51 (8–9), 883–915.

Nahon, A., Bertin, X., Fortunato, A.B., Oliveira, A., 2012. Process-based 2dh morphodynamic modeling of tidal inlets: a comparison with empirical classifications and theories. Mar. Geol. 291, 1–11.
O'Brien, M.P., 1931. Estuary tidal prisms related to entrance areas. Civ. Eng. 1 (8), 738–739.
O'Brien, M.P., 1969. Equilibrium flow areas of tidal inlets on sandy coasts. J. Waterw. Harbors 95, 43–52.
Oost, A.P., 1995. Dynamics and sedimentary developments of the Dutch Wadden Sea with a special emphasis on the Frisian Inlet: a study of the barrier islands, ebb-tidal deltas, inlets and drainage basins. Faculteit Aardwetenschappen.
Ridderinkhof, W., de Swart, H.E., van der Vegt, M., Hoekstra, P., 2014. Influence of the back-barrier basin length on the geometry of ebb-tidal deltas. Ocean Dynam. 64 (9), 1333–1348.
Ridderinkhof, W., de Swart, H.E., van der Vegt, M., Hoekstra, P., 2016a. Modeling the growth and migration of sandy shoals on ebb-tidal deltas. J. Geophys. Res.: Earth Surf. 121 (7), 1351–1372.
Ridderinkhof, W., Hoekstra, P., van der Vegt, M., de Swart, H.E., 2016b. Cyclic behavior of sandy shoals on the ebb-tidal deltas of the wadden sea. Continent. Shelf Res. 115, 14–26.
Ris, R.C., Holthuijsen, L.H., Booij, N., 1999. A third-generation wave model for coastal regions: 2. verification. J. Geophys. Res.: Oceans 104 (C4), 7667–7681.
Rizzetto, F., Tosi, L., Zecchin, M., Brancolini, G., Baradello, L., Tang, C., et al., 2009. Ancient geomorphological features in shallows of the venice lagoon (Italy). J. Coast Res. 56 (Special Issue), 752–756.
Roelvink, J., 2006. Coastal morphodynamic evolution techniques. Coast. Eng. 53 (2–3), 277–287.
Sennes, G., Castelle, B., Bertin, X., Mirfenderesk, H., Tomlinson, R., 2007. Modelling of the gold coast seaway tidal inlet, Australia. J. Coast Res. 1086–1091.
Sha, L., 1990. Surface sediments and sequence models in the ebb-tidal delta of texel inlet, wadden sea, The Netherlands. Sediment. Geol. 68 (1–2), 125–141.
Stutz, M.L., Pilkey, O.H., 2005. The relative influence of humans on barrier islands: humans versus geomorphology. Hum. Geol. Agents 16, 137.
Van de Kreeke, J., 2006. An aggregate model for the adaptation of the morphology and sand bypassing after basin reduction of the Frisian inlet. Coast. Eng. 53 (2–3), 255–263.
Van der Spek, A.J., 2018. The development of the tidal basins in the Dutch wadden sea until 2100: the impact of accelerated sea-level rise and subsidence on their sediment budget–a synthesis. Neth. J. Geosci. 97 (3), 71–78.
Van Rijn, L., Walstra, D., Ormondt, M.v., 2004. Description of Transpor2004 and Implementation in Delft3d-Online: Final Report. Technical report, Deltares (WL).
Vermeersen, B.L., Slangen, A.B., Gerkema, T., Baart, F., Cohen, K.M., Dangendorf, S., Duran-Matute, M., Frederikse, T., Grinsted, A., Hijma, M.P., et al., 2018. Sea-level change in the Dutch wadden sea. Neth. J. Geosci. 97 (3), 79–127.
Walton, T.L., Adams, W.D., 1976. Capacity of inlet outer bars to store sand. Coast. Eng. Proc. 1 (15).
Wang, Y.-H., Tang, L.-Q., Wang, C.-H., Liu, C.-J., Dong, Z.-D., 2014. Combined effects of channel dredging, land reclamation and long-range jetties upon the long-term evolution of channel-shoal system in qinzhou bay, sw China. Ocean Eng. 91, 340–349.
Wang, Z.B., Elias, E.P., van der Spek, A.J., Lodder, Q.J., 2018. Sediment budget and morphological development of the Dutch wadden sea: impact of accelerated sea-level rise and subsidence until 2100. Neth. J. Geosci. 97 (3), 183–214.
Zhou, Z., Coco, G., van der Wegen, M., Gong, Z., Zhang, C., Townend, I., 2015. Modeling sorting dynamics of cohesive and non-cohesive sediments on intertidal flats under the effect of tides and wind waves. Continent. Shelf Res. 104, 76–91.